The F-BAR protein CIP4 promotes GLUT4 endocytosis through bidirectional interactions with N-WASp and Dynamin-2

Sean M. Hartig[1,2], Shuhei Ishikura[3], Rachel S. Hicklen[1], Yanming Feng[1,4], Elisabeth G. Blanchard[1], Kevin A. Voelker[5], Christina S. Pichot[1], Robert W. Grange[5], Robert M. Raphael[6], Amira Klip[3] and Seth J. Corey[1,4,*]

[1]Division of Pediatrics, University of Texas MD Anderson Cancer Center, Houston, TX 77030, USA
[2]Department of Molecular and Cellular Biology, Baylor College of Medicine, Houston, TX 77030, USA
[3]Cell Biology Program, Hospital for Sick Children, Toronto, ON, M5G 1X8, Canada
[4]Department of Pediatrics, Northwestern University Feinberg School of Medicine, Chicago, IL 60611, USA
[5]Department of Human Nutrition, Foods and Exercise, Virginia Polytechnic Institute and State University, Blacksburg, VA 24061, USA
[6]Department of Bioengineering, Rice University, Houston, TX 77005, USA
*Author for correspondence (e-mail: s-corey@northwestern.edu)

Accepted 31 March 2009
Journal of Cell Science 122, 2283-2291 Published by The Company of Biologists 2009
doi:10.1242/jcs.041343

Summary

F-BAR proteins are a newly described family of proteins with unknown physiological significance. Because F-BAR proteins, including Cdc42 interacting protein-4 (CIP4), drive membrane deformation and affect endocytosis, we investigated the role of CIP4 in GLUT4 traffic by flow cytometry in GLUT4myc-expressing L6 myoblasts (L6 GLUT4myc). L6 GLUT4myc cells express CIP4a as the predominant F-BAR protein. siRNA knockdown of CIP4 increased insulin-stimulated ^{14}C-deoxyglucose uptake by elevating cell-surface GLUT4. Enhanced surface GLUT4 was due to decreased endocytosis, which correlated with lower transferrin internalization. Immunoprecipitation of endogenous CIP4 revealed that CIP4 interacted with N-WASp and Dynamin-2 in an insulin-dependent manner. FRET confirmed the insulin-dependent, subcellular properties of these interactions. Insulin exposure stimulated specific interactions in plasma membrane and cytosolic compartments, followed by a steady-state response that underlies the coordination of proteins needed for GLUT4 traffic. Our findings reveal a physiological function for F-BAR proteins, supporting a previously unrecognized role for the F-BAR protein CIP4 in GLUT4 endocytosis, and show that interactions between CIP4 and Dynamin-2 and between CIP4 and NWASp are spatially coordinated to promote function.

Supplementary material available online at
http://jcs.biologists.org/cgi/content/full/122/13/2283/DC1

Key words: F-BAR, N-WASp, Endocytosis

Introduction

Dynamic cytoskeletal organization underlies many diverse cellular processes, including vesicle traffic and membrane deformation. Key components of actin cytoskeletal assembly are the RhoGTPases Cdc42, Rac, and Rho (Hall, 1998), the Arp2/3 activator N-WASp (Higgs and Pollard, 2001), and scaffolding proteins such as cortactin (Weaver et al., 2001). With either activated Cdc42 or the non-catalytic domains of the Src kinase Lyn as bait, yeast two-hybrid screens isolated a novel adaptor protein, Cdc42 interacting protein-4 (CIP4) (Aspenstrom, 1997; Dombrosky-Ferlan et al., 2003). CIP4 is an F-BAR protein with a hydrophobic, N-terminal alpha-helical region related to Bin Amphiphysin Rvs (BAR) family proteins. These proteins bridge actin to the lipid bilayer, promoting plasma membrane remodeling (Itoh and De Camilli, 2006; Tsujita et al., 2006). Most F-BAR proteins contain at least one C-terminal SH3 domain, facilitating interactions with proline-rich proteins like N-WASp and the GTPase dynamin (Kamioka et al., 2004; Tian et al., 2000). The SH3 domain of several F-BAR proteins has been reported to function in endocytosis (Itoh et al., 2005; Kessels and Qualmann, 2002; Tsujita et al., 2006). Other members of the F-BAR family closely related to CIP4 are transducer of Cdc42-dependent actin assembly-1 (Toca-1) (Ho et al., 2004) and formin binding protein-17 (FBP-17), but do not yet have established physiologic functions. However, biochemical studies have shown that Toca-1 is a critical factor in N-WASp-dependent activation of actin nucleation (Ho et al., 2004), whereas FBP17 induces tubular membrane invagination (Kamioka et al., 2004).

Glucose uptake in muscle and adipose tissues is regulated by tuning the amount of GLUT4 at the plasma membrane (Dugani and Klip, 2005; Watson et al., 2004). GLUT4 traffic between intracellular compartments and the plasma membrane is tightly controlled by insulin. Insulin acts to acutely increase the amount of plasma membrane GLUT4 by increasing exocytosis and, in adipocytes, by decreasing endocytosis through both phosphoinositide-3-kinase (PI3K)-dependent and independent signaling pathways. The mechanism of GLUT4 endocytosis is still poorly understood, although previous studies have established cholesterol-, dynamin- and clathrin-dependent routes (Al-Hasani et al., 1998; Antonescu et al., 2008; Blot and McGraw, 2006; Robinson et al., 1992).

An alternate splice form of CIP4 (CIP4h or CIP4/2) was identified in a yeast two-hybrid screen of a 3T3L1 adipocyte cDNA library with the RhoGTPase TC10 as bait (Chang et al., 2002). In these cells, insulin-dependent GTP-loading of TC10 in adipocytes leads to recruitment and interactions with several proteins, including CIP4h, that function as a multi-component scaffold to promote the traffic of

GLUT4 to the cell surface (Chang et al., 2004). However, whether the translocation of CIP4 to the plasma membrane can contribute to GLUT4 endocytosis has yet to be investigated. Furthermore, the subcellular and spatial coordination of SH3-dependent interactions between CIP4, N-WASp and Dynamin-2 to promote vesicle traffic is largely undefined because previous studies have focused on immunoprecipitation under conditions of protein overexpression. In this study, we analyzed the role of CIP4 in insulin-dependent steady-state distribution and internalization of GLUT4myc in L6 GLUT4myc myoblasts through a cell-population-based assay (Wang et al., 1998) adapted for flow cytometry. Our data suggest that interactions between CIP4, N-WASp and Dynamin-2 are governed by subcellular localization and indicate that CIP4 negatively regulates glucose uptake by promoting GLUT4 endocytosis in muscle cells, further defining a physiologic role for F-BAR proteins.

Results

CIP4a is the most predominant F-BAR protein in L6 GLUT4myc cells

Two predominant splice isoforms of CIP4 have been reported: the ubiquitously present CIP4a (Aspenstrom, 1997) and CIP4h (Wang et al., 2002), also called CIP4/2 (Chang et al., 2002), which is expressed predominantly in the heart. CIP4h contains an extra exon encoding 56 amino acids responsible for binding the activated form of TC10 (Chang et al., 2002). Therefore, we analyzed the expression levels of CIP4a in comparison with two other closely related F-BAR proteins, FBP17 and Toca-1, in the rat skeletal muscle cell line, L6 GLUT4myc, which contains an epitope tag in the first exofacial loop of GLUT4 to allow for surface detection (Wang et al., 1998). Using quantitative PCR (qPCR) primers specific for CIP4a, CIP4h, FBP17 and Toca-1, CIP4a was found to be the most highly expressed F-BAR protein compared to these two other very similar family members (Fig. 1A). More specifically, CIP4a has an approximately tenfold higher expression level than FBP17 and Toca-1, which share similar transcript levels in the L6 GLUT4myc myoblasts. Furthermore, CIP4a mRNA is ten times more abundant than CIP4h. At the protein level, by immunoblot we used an antibody that detects CIP4a and CIP4h isoforms at approximately 75 and 85 kDa, respectively (Fig. 1B). CIP4a, with a band migrating at the same mobility as the CIP4a positive control, was the most predominant isoform of CIP4, whereas CIP4h was not detected. In agreement with previously published results (Tsujita et al., 2006), when CIP4 was knocked by siRNA, no compensatory increase in FBP17 was detected by western blotting and qPCR (data not shown).

CIP4 colocalizes with GLUT4 and negatively regulates glucose uptake without alterations in insulin-responsive Akt signaling

To study the role of endogenous CIP4a in the regulation of glucose transport and insulin signaling in skeletal muscle cells, CIP4a expression was reduced by RNAi. L6 GLUT4myc cells were transfected with vehicle, CIP4-specific, or mismatch control RNAi. The depletion of CIP4 in L6 GLUT4myc cells enhanced insulin-stimulated glucose uptake by 1.4-fold over the mock or scrambled controls (Fig. 2A). Furthermore, CIP4a knockdown did not affect insulin-dependent Akt phosphorylation (Fig. 2B). This profile indicated that CIP4 negatively regulated insulin-mediated glucose uptake without disrupting Akt-PKB signaling nodes.

The effects of insulin stimulation on L6 myoblasts were analyzed to confirm the findings that CIP4 colocalizes with GLUT4 in 3T3L1 adipocytes (Chang et al., 2002). In the basal state, CIP4 was present throughout the cell, whereas insulin stimulation showed plasma membrane localization of CIP4 and GLUT4 in L6 GLUT4myc cells (Fig. 3A). However, only a small population of CIP4 translocates to the cell surface in response to insulin. These results were extended to primary murine tissue (supplementary material Fig. S1). Age- and sex-matched mice were starved overnight and challenged with glucose. Muscle (Extensor Digitorum Longus) tissue was collected, formalin fixed, and sections prepared. Antibody staining for CIP4 and GLUT4 verified findings established in the L6 GLUT4myc. To determine whether the localization of CIP4 was unique, further experiments were performed using an antibody to FBP17 (Fig. 3B). After stimulation with insulin, the FBP17 distribution remains diffuse without any colocalization with GLUT4. This finding establishes a potential non-redundant role for CIP4 in the maintenance of GLUT4 traffic.

Insulin induces dynamic interactions between CIP4, N-WASp and Dynamin-2 that underlie the GLUT4 response

We hypothesized that the increased glucose uptake due to downregulation of CIP4 expression resulted from increased cell-surface GLUT4. To validate this hypothesis we again reduced endogenous CIP4 via RNAi in L6 GLUT4myc cells. The translocation of GLUT4myc allowed for direct staining and the quantification of the surface GLUT4 by flow cytometry. No significant differences ($P>0.05$) were seen in basal GLUT4myc staining amongst all conditions. After insulin stimulation, however, CIP4-deficient cells exhibited a 2.6-fold increase in cell surface GLUT4myc compared to the vehicle basal level (Fig. 4A). Controls, which were either vehicle transfected or treated with mismatched RNAi, did not yield significant differences in insulin-dependent GLUT4myc staining; insulin caused a 1.4-fold increase in surface GLUT4. Previous experiments with this cell line, through ELISA-based or confocal immunofluorescence of GLUT4myc, have established a twofold increase in surface GLUT4 after insulin stimulation (Ishikura and Klip, 2008; Wang et al., 1998). By this flow cytometric assay, a 40% increase in surface GLUT4 was detected for control RNA and vehicle transfections, allowing a qualitative detection of changes in surface GLUT4myc and an effect

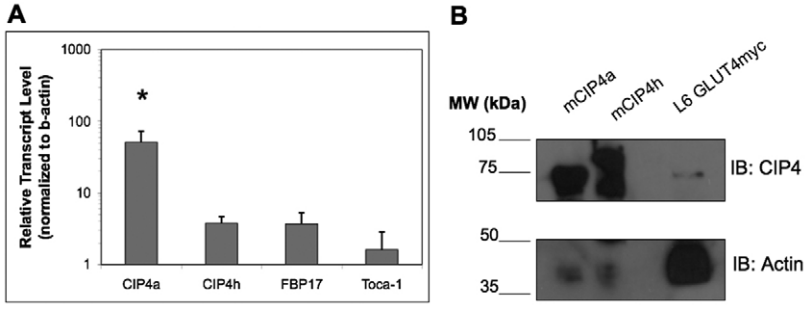

Fig. 1. CIP4 is highly expressed in L6 GLUT4myc myoblasts. (A) RNA was isolated and transcript levels were evaluated by quantitative PCR using primers specific for CIP4a, CIP4h, FBP17, and Toca-1. Values represent means ± s.e.m. $n=4$, $^*P<0.05$. (B) CIP4a is the predominant CIP4 isoform present as detected by western blot. Lysates were prepared from L6 GLUT4myc myoblasts, resolved by SDS-PAGE, transferred onto a PVDF membrane and immunoblotted for CIP4. Specific isoforms were identified by comparison to HEK293T cells transfected with plasmids encoding CIP4a and CIP4h.

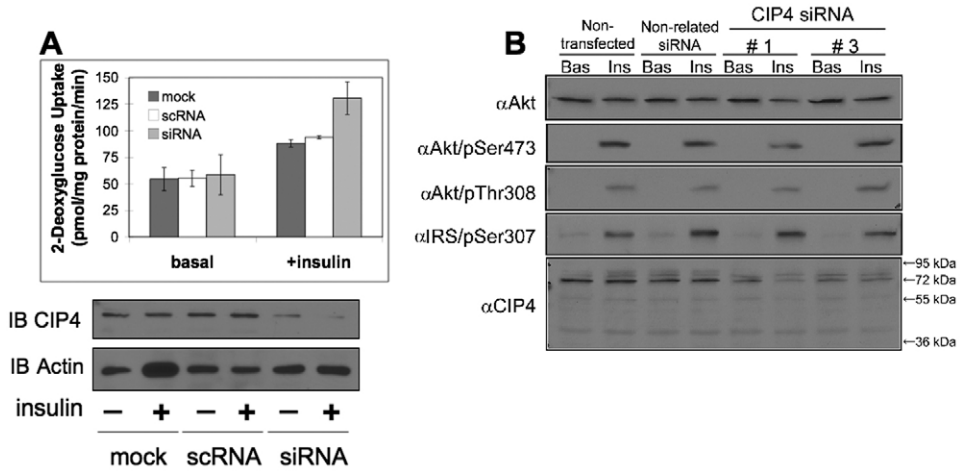

Fig. 2. Knockdown of CIP4 enhances glucose uptake without disrupting insulin-sensitive Akt-PKB signaling. (A) The insulin-mediated uptake of 2-deoxyglucose was measured by serum and glucose starvation of siRNA-treated L6 myoblasts followed by stimulation with 100 nM insulin for 15 minutes. Subsequent to the 15 minute stimulus, [^{14}C]2-deoxy-D-glucose was added at a final concentration of 0.6 µCi/ml for a further 5 minutes. Cells were then lysed for protein normalization and collected for scintillation counting. Basal indicates cultures without insulin stimulation. Values represent means ± s.e.m. *n*=3. (B) Components of the Akt insulin-dependent signaling pathway were immunoblotted in rat L6 myoblasts. Rat L6 myoblasts were treated with CIP4 siRNA (or mismatched control) and stimulated with insulin for 20 minutes after at least a 3-hour serum-free starvation. Whole-cell lysates were prepared and blotted for components of the Akt-PKB insulin-sensitive signaling pathway.

regulated by CIP4. Therefore, these data indicated that absence of CIP4 results in greater surface expression of GLUT4 and leads to the increased glucose uptake observed in Fig. 2A.

Due to the importance of the SH3 domain of CIP4 and F-BAR domains in endocytosis (Itoh et al., 2005; Kessels and Qualmann, 2002; Tsujita et al., 2006), interactions with Dynamin-2 and N-WASp were examined. Both proline-rich proteins have been found to interact with F-BAR proteins through SH3 domains, including CIP4 (Itoh et al., 2005; Kessels and Qualmann, 2002; Tian et al., 2000; Tsujita et al., 2006), and are important for GLUT4 traffic (Al-Hasani et al., 1998; Jiang et al., 2002). Verification of an interaction between the SH3 domain of CIP4a with Dynamin-2 and N-WASp was evaluated by GST-SH3 pull-down assays with lysates from untransfected L6 GLUT4myc cells. As shown in Fig. 4B, the SH3 domain of CIP4 binds both Dynamin-2 and N-WASp, suggesting that these interactions might be needed for GLUT4 endocytosis.

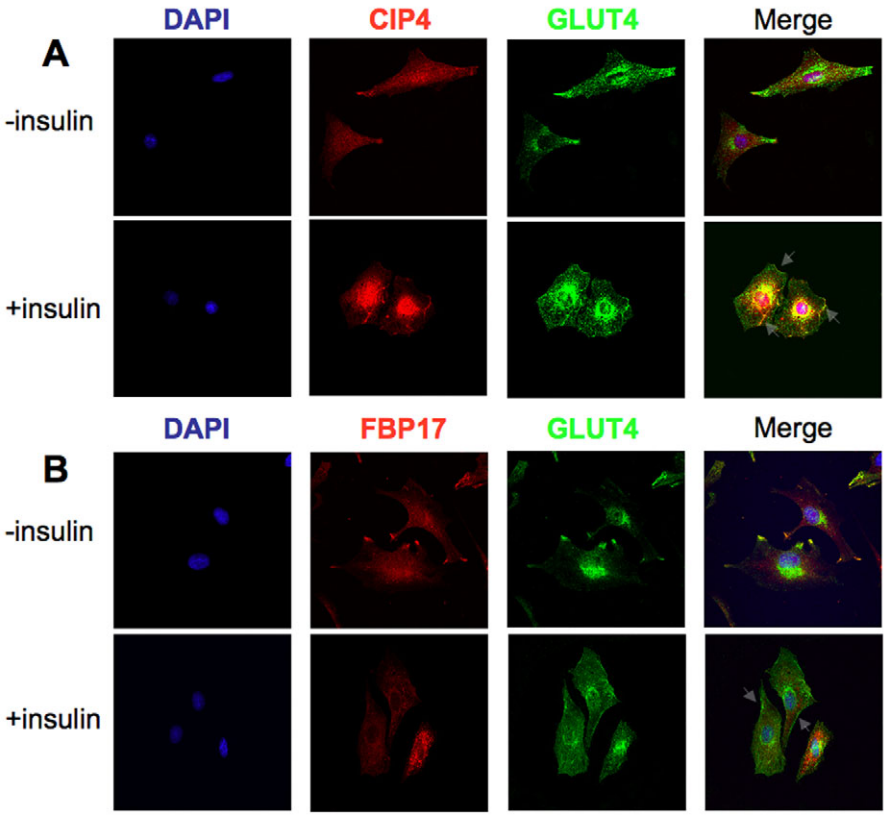

Fig. 3. Insulin directs a localization of CIP4 and GLUT4. L6 GLUT4myc myoblasts were starved for 3-5 hours with or without 100 nM insulin. Following treatment, the localizations of (A) CIP4 and GLUT4 or (B) FBP17 and GLUT4 were determined by immunofluorescence with appropriate antibodies.

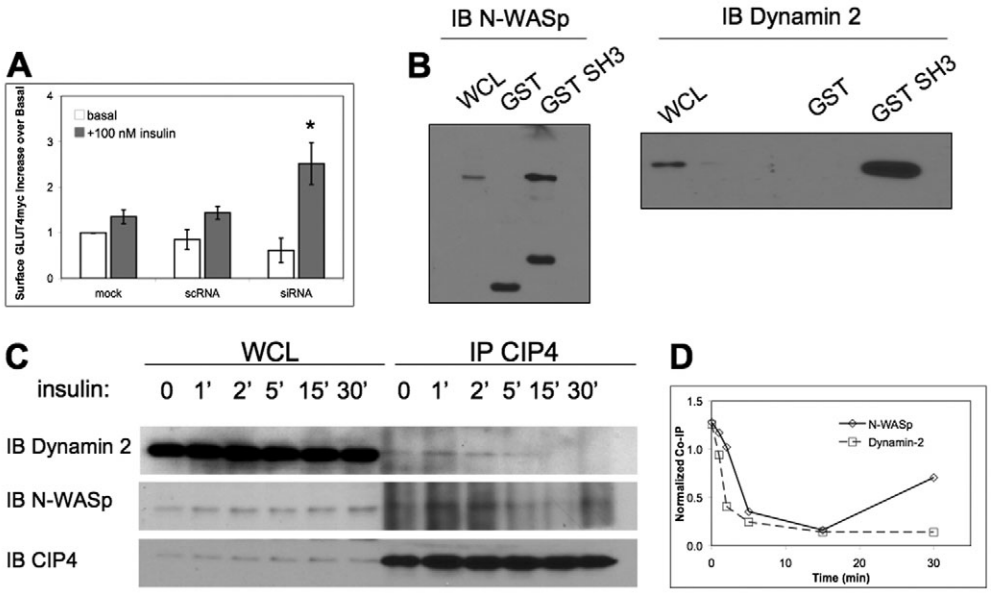

Fig. 4. CIP4 negatively regulates surface GLUT4 and participates in insulin-dependent interactions through its SH3 domain. (A) Rat L6 GLUT4myc myoblasts were treated with siRNA to CIP4, scrambled control or vehicle alone (mock). Upper panel indicates the ratio of insulin-treated to untreated cell surface expression of myc-tagged GLUT4 as detected by flow cytometry. All values are normalized to mock transfected cultures and represent means ± s.e.m. n=3, *P<0.05. (B) Immobilized GST CIP4-SH3 and GST were incubated with lysates of untransfected L6 GLUT4myc myoblasts. Pull-down products were immunoblotted for either N-WASp or Dynamin-2 in separate experiments. (C) L6 GLUT4myc cells were serum-starved for 5 hours and stimulated with 100 nM insulin for the times indicated. Cells were lysed at each time point and CIP4 was immunoprecipitated with a monoclonal anti-CIP4 antibody. Immunoprecipitates were blotted for Dynamin-2 and N-WASp, and reprobed for CIP4. The experiment shown is representative of two independent experiments. (D) Intensities of bands at each time-point were measured with ImageJ and normalized to the CIP4 input.

As shown in Fig. 4C, the associations between CIP4 and Dynamin-2 and between CIP4 and N-WASp were evaluated by immunoprecipitation of endogenous CIP4 from L6 GLUT4myc cells during the time-course of insulin stimulation. The resulting kinetic CIP4 immunoprecipitations revealed that the association of CIP4 with N-WASp and Dynamin-2 was quite dynamic. CIP4 interacted with both N-WASp and Dynamin-2 after 5 hours of starvation, followed by a steady degradation in interaction after insulin stimulation. The Dynamin-2 association then appeared to precipitously decrease whereas the N-WASp interaction was sustained, and even increased at 30 minutes, indicated by the normalization of each band to immunoprecipitation input (Fig. 4D).

Spatial dynamics of insulin-dependent interactions between CIP4 and N-WASp and between CIP4 and Dynamin-2

The associations between CIP4 and N-WASp and between CIP4 and Dynamin-2 under insulin stimulation (demonstrated in Fig. 4C) were further investigated by acceptor photobleach FRET (apFRET). This method allowed us to monitor the spatial modulations in association between CIP4 and these two binding partners at resolutions not possible by standard immunofluorescence imaging or immunoprecipitation and western blotting. The application of apFRET involves bleaching the acceptor population in a region of the cell and measuring the subsequent increase in donor fluorescence due to dequenching of the energy transfer (Bastiaens and Jovin, 1996; Karpova et al., 2003). For this approach, we analyzed membrane and cytosolic FRET efficiencies for L6 GLUT4myc cells co-transfected with YFP CIP4a and CFP Dynamin-2 or CFP N-WASp. As shown in Fig. 5A-B (upper panels), expression of these plasmids results in a diffuse localization. apFRET measurements were made by collecting a pre-bleach image and creating regions of interest (ROIs) for data acquisition. Fig. 5A-B represents the method applied where ROI 3 is the entire scanning region, ROI 4 a control region, followed by ROI 1 and ROI 2 as membrane and cytosolic compartments, respectively. After photobleaching of YFP fluorescence in ROI 1 and ROI 2, post-bleach images (Fig. 5A-B, lower panels) were acquired and analyzed. The increases in FRET efficiency between CIP4–Dynamin-2 and CIP4–N-WASp were verified by evaluating several negative controls (Table 1). As shown, FRET efficiencies measured between these two pairs described specific protein interactions.

Table 1. apFRET analysis of control and experimental conditions in L6 GLUT4myc myoblasts

Plasmid	None	CFP	CFP N-WASp	CFP Dynamin-2
None	–	–	4.9±1.6	5.1±4.7
YFP	–	–	8.6±1.7	5.5±2.1
YFP CIP4	–2.54±0.23	6.0±1.8	14.7±1.5 to 30.7±2.3	8.9±1.7 to 19.7±1.8

Control experiments were performed with appropriate plasmids to verify the specificity of interactions between YFP CIP4 and CFP Dynamin-2 and between YFP CIP4 and CFP N-WASp. Photobleach parameters were applied as denoted in the Materials and Methods. Each value is the mean of at least seven measurements ± s.e.m.

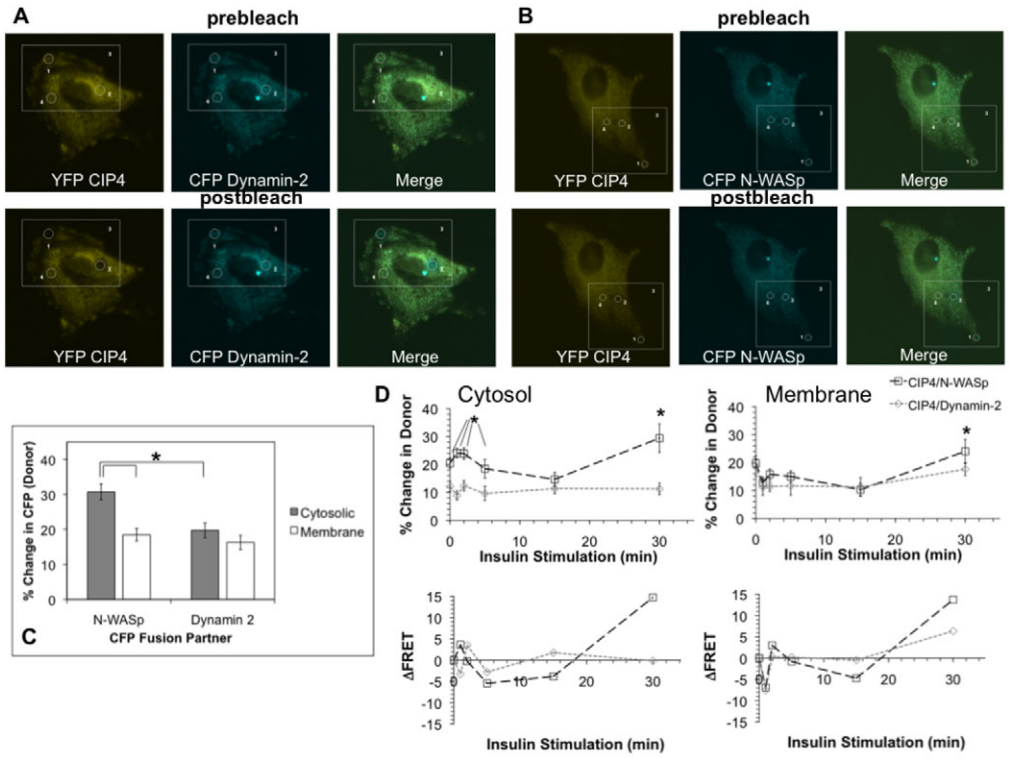

Fig. 5. Kinetic and spatiotemporal assessment of CIP4–Dynamin-2 and CIP4–N-WASp insulin-dependent interactions by apFRET. Representative images are shown for L6 GLUT4myc co-transfected with (A) YFP CIP4 or CFP Dynamin-2 or (B) YFP CIP4 or CFP N-WASp. ROIs for photobleaching were defined for membrane (ROI 1) and cytosolic (ROI 2) regions. Control (ROI 3) and scanning (ROI 4) regions were also defined to assess the extent of off-target bleaching. (C) Increases in donor (CFP) intensity after acceptor (YFP) photobleaching of subcellular compartments were measured for cells under standard culture conditions. All values are presented as mean ± s.e.m. for a minimum of 12 measurements. The asterisk indicates linked, statistically different pairs (P<0.05). (D) Dynamic changes in protein-protein interactions were assessed by apFRET during insulin stimulation of L6 GLUT4myc myoblasts. Cells were starved for 5 hours and exposed to 100 nM insulin for the times indicated. After each time-point, specimens were fixed in 4% paraformaldehyde and mounted for apFRET. Following collection of all data points for both co-transfection conditions rates, changes in FRET efficiency between fluorophores were calculated as described in the Materials and Methods. Time-course data were further transformed into derivative representations. Each time-point is a minimum of 11 measurements ± s.e.m. Asterisks indicate statistically different pairs of means (P<0.05).

For cells maintained under standard culture conditions, plasma membrane FRET efficiencies were statistically equivalent for both co-transfections, whereas CIP4–N-WASp cytosolic donor dequenching was significantly greater than that of CIP4–Dynamin-2 (Fig. 5C). This indicates that a higher extent of interaction exists between CIP4 and N-WASp under quiescent conditions.

apFRET was further applied to understand the insulin-mediated, subcellular behavior not resolvable by the immunoprecipitations in Fig. 4C. As shown in Fig. 5D (upper panels), increases in FRET efficiencies immediately occurred between these two pairs of fusion proteins upon insulin exposure. For cytosolic bleaches, a peak in the N-WASp–CIP4 interaction was detected after 1 minute of stimulation. Subsequently, a peak was measured for Dynamin-2–CIP4 at 2 minutes of insulin addition. Membrane FRET efficiencies were less dynamic than intracellular measurements; a maximum in both interactions was observed at 2 minutes with a steady state level of interaction between these pairs of fusion proteins occurring at later time-points. In both compartments, longer time-points resulted in steady-state regimes. Because FRET represents an intermolecular distance between fluorophores, the efficiencies were qualitatively transformed into distances and derivative plots constructed for membrane and cytosolic observations (Fig. 5D, lower panels). These observations provided further insight to the temporal pattern of these interactions and displayed the differences between membrane and intracellular efficiencies. Together, they support the suggestion that CIP4 functions as an adapter protein linking its binding partners to specific functions in different cellular regions.

CIP4 promotes both GLUT4 and transferrin endocytosis

Specific effects on GLUT4 endocytosis were decoupled from steady-state GLUT4myc measurements to determine the mechanism of increased surface GLUT4 when CIP4 expression was disrupted (Fig. 4A). In this approach, cells were transfected with RNAi in combination with vector control (EGFP) or EGFP dynamin 1 K44A, where the K44A mutation functions as a dominant negative inhibitor of GLUT4 endocytosis (Al-Hasani et al., 1998; Antonescu et al., 2008; Volchuk et al., 1998). Two days later, L6 GLUT4myc cells were stimulated with insulin for 10 minutes to translocate GLUT4myc to the cell surface. The exofacial myc epitope was then bound with antibody at 4°C, followed by warming the cells in the presence or absence of insulin for a further 10 minutes. The extent of disappearance of antibody-myc complexes was then measured after secondary antibody binding and compared to that in cultures continuously maintained at 4°C. Upon CIP4 knockdown, GLUT4myc was largely retained at the cell surface, establishing the role of CIP4 as a positive regulator of GLUT4 endocytosis (Fig. 6A). In agreement with previous studies, GLUT4 internalization

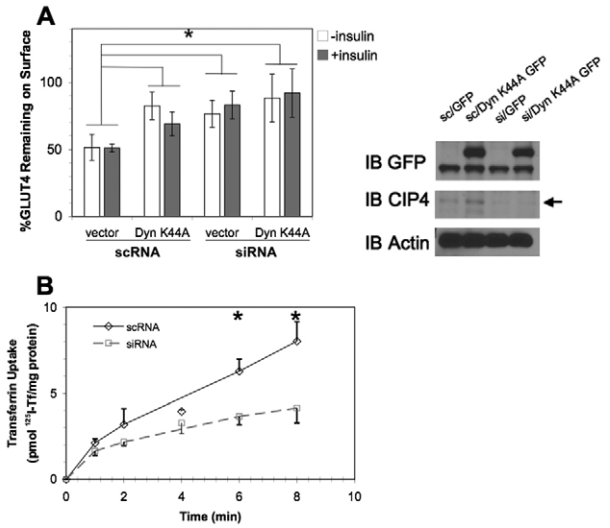

Fig. 6. GLUT4 and transferrin endocytosis are promoted by CIP4. (A) L6 GLUT4 myc were cotransfected with scrambled siRNA (scRNA) or CIP4-specfic siRNA (siRNA) in combination with dynamin-1 K44A EGFP (dyn K44A) or the GFP vector control (vector). After 48 hours, the cells were stimulated with 100 nM insulin for 10 minutes and chilled to 4°C. Surface GLUT4-myc was labeled with anti-myc antibody followed by extensive washing with PBS. Cells were then warmed to 37°C in the presence or absence of insulin for 15 minutes. Subsequently, cells were again cooled to 4°C and incubated with goat anti-mouse IgG $F(ab')_2$ to detect persisting primary antibody-GLUT4myc complexes on the cell surface. Surface GLUT4 was then determined by flow cytometry as described in the Materials and Methods. Error bars represent the mean ± s.e.m. for a minimum of three measurements. All values differ significantly from the scrambled vector control (*P<0.05). Panels on the right display western blots for RNAi-dynamin cotransfections. (B) The effect of CIP4 knockdown on transferrin endocytosis in L6 GLUT4myc was determined by serum starvation and stimulation with a saturating concentration of ^{125}I transferrin for the indicated times (n=3). Asterisks indicate means that differ significantly from the scrambled vector control (P<0.05).

was found to be dynamin-dependent (Al-Hasani et al., 1998; Antonescu et al., 2008; Volchuk et al., 1998). Additionally, CIP4 knockdown resulted in a similar amount of latent surface GLUT4, indicative of a cooperativity of CIP4 and Dynamin to promote GLUT4 endocytosis. These results were comparable in the presence or absence of insulin, suggesting that insulin does not alter the rate of GLUT4 endocytosis.

The requirement for CIP4 in clathrin-mediated endocytosis of transferrin was studied by incubating L6 GLUT4myc cells (Fig. 6B) with ^{125}I-transferrin. Transferrin uptake was significantly inhibited when CIP4 was knocked down at later time-points, both 6 minutes (–42%) and 8 minutes (–49%), compared to scrambled control. This finding was consistent with the recently reported role of F-BAR proteins in endocytosis of EGF after RNAi silencing of CIP4 and/or FBP17 in A431 cells (Tsujita et al., 2006) and transferrin in COS-7 cells (Itoh et al., 2005).

Discussion

Endocytosis requires multiple, highly coordinated, spatiotemporal, biophysical and biochemical events that perturb the membrane bilayer and require cytoskeletal reorganization. A newly identified family of proteins, F-BAR, has been identified that functions in membrane dynamics and links lipid bilayer perturbations to the actin cytoskeleton (Itoh et al., 2005; Tsujita et al., 2006). An isomeric variant of these proteins, CIP4h (also known as CIP4/2), has been found to function directly with the insulin-regulated GTPase TC10 to direct GLUT4 to the cell surface in adipocytes (Chang et al., 2002; Chang et al., 2007; Lodhi et al., 2007). Additionally, Lodhi et al. proposed that CIP4 and a proline-rich GTP-exchange factor, Gapex-5, form a complex and maintain the internal compartmentalization of GLUT4 within endosomal vesicles. Insulin treatment promotes the translocation of CIP4–Gapex-5 to the plasma membrane and release of GLUT4 from internal storage vesicles of fat cells (Lodhi et al., 2007). In contrast to these findings, CIP4h was far less expressed in muscle cells at both the transcript and protein levels (Fig. 1). Instead, a survey of the CIP4 family of F-BAR proteins in L6 GLUT4myc cells showed that CIP4a, which does not contain the TC10 binding domain, was the most highly expressed by q-PCR. Knockdown of CIP4a did not result in alterations in Akt-dependent signaling, leading to the conclusion that CIP4a-mediated GLUT4 traffic, like its splice variant CIP4h, is regulated by alternative upstream signals.

RNAi silencing of CIP4a resulted in increased insulin-stimulated glucose uptake. The glucose uptake was potentiated by an increase in surface GLUT4, which was due to a slower endocytic rate. The endocytosis defect caused by CIP4 RNAi was comparable to co-transfection of a dominant negative dynamin, indicating that CIP4 and dynamin function to promote internalization through the same pathway, as previously established by Itoh et al. (Itoh et al., 2005). Transferrin internalization was also inhibited, implicating the role of CIP4a in a more general endocytic phenomena.

Other recent studies suggest a role for Gapex-5 (and hence CIP4) in endocytosis. In investigating the role of Gapex-5 on epidermal growth factor receptor (EGFR) traffic, Su et al. (Su et al., 2007) found that Gapex-5 RNAi resulted in decreased EGFR degradation. Therefore, not only must the interaction of CIP4 with Gapex-5 contribute to the membrane targeting of GLUT4, but it might also function in its internalization. Several recent publications focused on the BAR proteins SNX4 and Amphiphysin describe pleiotropic functions for these proteins whereby they not only promote endocytosis, but also the endosomal sorting of transferrin receptors (Leprince et al., 2003; Traer et al., 2007)

Through its SH3 domain, CIP4 interacts with both N-WASp and Dynamin-2 to link actin polymerization and membrane deformation, respectively, to promote GLUT4 traffic. This interaction has been extensively defined through biochemical assays for BAR and F-BAR proteins, including amphiphysin (Wigge et al., 1997), SNX9 (Badour et al., 2007; Lundmark and Carlsson, 2003) syndapins (Kessels and Qualmann, 2002), Nostrin (Icking et al., 2005), Toca-1 (Kakimoto et al., 2006) and FBP17 (Kamioka et al., 2004). Novel to this study was a further understanding of these interactions by immunoprecipitation, without overexpression of any protein, and through apFRET. We have characterized the time-course of these interactions and shown that specific cellular compartments contribute to the dynamics of insulin-mediated associations between CIP4 and Dynamin-2 and between CIP4 and N-WASp. These findings provide evidence for the following two interpretations. In the cytosolic compartment during insulin stimulation, N-WASp interacts with CIP4 early, followed by a potential displacement of the SH3 domain of CIP4 by Dynamin-2. Membranous CIP4 functioned more like a scaffold protein, whereby N-WASp and Dynamin-2 move away from CIP4 to potentially bind the Arp2/3 complex or provide constriction to growing endocytic pits. The in-phase pattern of the data also favors models of head-to-head F-BAR dimerization (Henne et al., 2007), whereby SH3 domains are

exposed for simultaneous binding of N-WASp and Dynamin (Fig. 5D). In support of our observations, recent evidence has also shown periodic activity of N-WASp and Dynamin during clathrin-mediated endocytosis (Merrifield et al., 2002; Merrifield et al., 2005).

Recent studies (Itoh et al., 2005; Tsujita et al., 2006) have raised this question of paralogous function amongst the F-BAR proteins. Yet, there are subtle differences in domain structure that separate FBP17, CIP4 and Toca-1. Amongst these proteins, there is a high degree of amino acid sequence homology in the F-BAR and SH3 domains. Overall, for the rat homologs, CIP4 shares approximately 64% sequence homology with both FBP17 and Toca-1, whereas Toca-1 and FBP17 share 74%. However, CIP4 (AA 420-479) diverges from Toca-1 (AA 480-533) in the ERM domain. The same is true for CIP4 (AA 414-473) and FBP17 (AA480-536); in that region FBP17 lacks the HR1 domain, which is present in both CIP4 and Toca-1. This establishes the potential for non-redundant action mediated by the domain between the F-BAR and SH3 domains.

Together, our findings support a previously unrecognized role for the F-BAR protein CIP4a in GLUT4 endocytosis. Further, the interactions between CIP4 and its binding partners, N-WASp and Dynamin-2, are spatially regulated by insulin treatment.

Materials and Methods

Antibodies and western blotting

The following antibodies were purchased from commercial sources: polyclonal dynamin 2 (Santa Cruz Biotechnology, Santa Cruz, CA), monoclonal CIP4 (BD Biosciences, San Jose, CA), polyclonal N-WASp (ECM Biosciences, Versailles, KY), actin (Santa Cruz Biotechnology), and monoclonal GFP (BD Biosciences). Immunoblotting for components of the Akt signaling pathway was performed with antibodies from Cell Signaling Technology (Danvers, MA): pAkt S473/T308, Akt, pIRS S307. An antibody to FBP17 was raised using a 20-amino-acid peptide specific to the mouse and human FBP17 sequence that shares no homology to Toca-1 or CIP4. The peptide was linked to keyhole limpet hemocyanin (KLH) and injected into New Zealand White Rabbits along with Complete Freund's Adjuvant. This was followed by several booster injections of the peptide along with Incomplete Freund's Adjuvant. Beginning with the fourth bleed, we began to see strong reactivity with FBP17 by western blot and immunofluorescence (Sigma-Genosys, The Woodlands, TX). Cultured cells were lysed in 1% NP-40 for 1 hour at 4°C, supplemented with appropriate protease and phosphatase inhibitors. Lysates were resolved by SDS-PAGE, transferred to PVDF membranes (Millipore, Billerica, MA), blocked in 5% milk and probed with specific antibodies. Membranes were washed in phosphate-buffered saline with 0.1% Tween, incubated with horseradish-peroxidase–conjugated secondary antibodies (Santa Cruz Biotechnology), and visualized by enhanced chemiluminescence (Western Lightning, Perkin-Elmer, Waltham, CA). Membranes were stripped by incubating in western blot stripping buffer (Restore, Pierce Biotechnology, Rockford, IL) at 37°C, and re-blocked in 5% milk for further probing.

Cell culture and transfection

Rat L6-GLUT4myc (L6 GLUT4myc) myoblasts were kindly provided by Amira Klip (Hospital for Sick Children, Toronto, Ontario, Canada) and maintained in cell monolayers with MEM-α supplemented with 10% FBS and 1 U/ml penicillin-streptomycin in a humidified atmosphere containing 5% CO_2 and 95% air at 37°C. Cells were grown in 10 cm dishes during routine culture followed by seeding to either eight-chamber microscopy slides (Lab-Tek II Chamber Slide System, Electron Microscopy Sciences, Hatfield, PA) or six-well plates for immunofluorescence or flow cytometry experiments. Prior to insulin stimulation (100 nM), 70% confluent myoblasts were starved for minimally 3 hours in serum-free MEM-α. Unless otherwise indicated, all transfections were carried out using Lipofectamine 2000 (Invitrogen, Carlsbad, CA) or calcium phosphate using the manufacturer's instructions. siRNA and mismatch control (Qiagen, Valencia, CA) oligomers or expression plasmids were incubated in antibiotic-free media for 24 hours (plasmids) or 48 hours (siRNA) before experimentation. Transfections were performed at approximately 70% cell confluency.

cDNA constructs and GST-pulldown assays

BL21 strain of *E. coli* was transformed with cDNA corresponding to the SH3 domain of CIP4 (aa 482-545) in the prokaryotic expression plasmid pGEX-4T1 (Pharmacia Biotech, Piscataway, NJ). GST or GST CIP4a-SH3 proteins were produced from large-scale bacterial growth following a 3-hour induction with 100 μM IPTG. GST fusion proteins immobilized on glutathione-agarose beads (Sigma, St Louis, MO) were incubated with untransfected rat L6 GLUT4myc myoblast lysates for 4 hours at 4°C and washed five times with 1% NP-40. Precipitated proteins were eluted with sample buffer and analyzed by western blotting. EGFP Dynamin 1 K44A was kindly provided by Pietro DeCamilli (Yale University, New Haven, CT). cDNAs for Dynamin-2 and N-WASp were provided by Mark McNiven (Mayo Clinic, Rochester MN) and Maddy Parsons (University of London, King's College, London, UK), respectively. Dynamin-2 and N-WASp were subcloned into AmCyan-C1 vectors (Clontech, Mountain View, CA). CIP4a was amplified by PCR and the PCR product subcloned into the pEYFP-N1 (Clontech) vector.

Immunoprecipitation

L6 GLUT4myc myoblasts were starved for 5 hours and stimulated with 100 nM insulin (Humulin, Eli Lilly, Chicago, IL) for 0 (starved continuously), 1, 2, 5, 15 and 30 minutes. Cells were quickly chilled to 4°C by successive washings with cold PBS on ice. Cultures were then gently scraped and lysed for 1 hour at 4°C in 1% NP-40 supplemented with protease and phosphatase inhibitors. Extracts were then clarified by centrifugation at 13,000 × ***g*** for 30 minutes and protein concentration determined by microBCA assay (Pierce Biotechnology). Samples containing 600 μg of total protein were immunoprecipitated overnight with monoclonal CIP4 antibody (1:200 concentration) followed by 6 hours of incubation at 4°C with protein G-Sepharose beads (Amersham Biosciences, Piscataway, NJ). The immunoprecipitates were extensively washed with lysis buffer, subjected to SDS-PAGE, and immunoblot analysis.

RNA isolation and quantitative PCR

Total cellular RNA was isolated from L6 GLUTmyc myoblasts using TRIzol Reagent (Invitrogen) according to the manufacturer's instructions. RNA was precipitated with isopropanol, reconstituted in 75% ethanol and stored at –20°C until cDNA synthesis. cDNA was synthesized from RNA by oligo-dT primed reverse transcription reaction (Promega, Madison, WI). cDNA was analyzed by real-time qPCR analysis performed using SYBR green (Bio-Rad, Hercules, CA) normalized to rat β-actin. PCR primers are summarized in supplementary material Table S1. Relative expression was assessed by the comparative cycle threshold method.

Glucose transport in L6 myoblasts

In six-well plates, RNAi-treated L6 GLUT4myc myoblasts were incubated at 37°C for 2 hours with DMEM containing 1% bovine serum albumin (BSA), and then washed with Krebs-Ringer buffer (130 mM NaCl, 5 mM KCl, 1.3 mM $CaCl_2$, 1.3 mM $MgSO_4$, 25 mM HEPES, pH 7.4). The cultures were further incubated without glucose in Krebs-Ringer buffer containing 1% BSA for 2 hours. Subsequently, cultures were stimulated with or without insulin (100 nM) for 15 minutes. Glucose uptake was initiated by addition of [^{14}C]2-deoxy-D-glucose (200 μCi/ml; GE Radiochemicals, Piscataway, NY) to a final assay concentration of 0.6 μCi/ml for a further 5 minutes. Transport was terminated by transferring cultures to ice followed by three washes with cold (4°C) PBS. The cells were solubilized with 0.05% SDS or 0.1% Triton-X100 and incorporated ^{14}C was determined by scintillation counting. Non-specific uptake and trapping in the extracellular space was determined by measuring uptake in the presence of 10 μM cytochalasin B (Biomol, Plymouth Meeting, PA). Specific uptake was normalized to total protein content as described (Moyers et al., 1996).

Flow cytometric detection of surface GLUT4 in rat L6 GLUT4myc myoblasts

Detection of steady-state surface GLUT4myc was analyzed through an adaptation of protocols described previously (Bogan et al., 2001; Wang et al., 1998). Transfected L6 GLUT4myc myoblasts in six-well plates, before and after insulin stimulation, were immediately transferred to ice, followed by cold-room washing three times with phophate-buffered saline containing $MgCl_2$ and $CaCl_2$ (PBS). Cells were blocked with 4% donkey serum and 2% BSA for 30 minutes at 4°C. The cultures were then incubated with primary antibody (anti c-myc 9E10, Santa Cruz Biotechnology) at a concentration of 1:100 for approximately 2 hours. Cells were again washed three times with PBS, followed by incubation with a 1:200 dilution of phycoerythrin (PE)-conjugated donkey $F(ab')_2$ anti-mouse IgG secondary antibody (Santa Cruz Biotechnology) for 1 hour, also at 4°C. GLUT4 endocytosis was analyzed by treating cells with 100 nM insulin for 10 minutes followed by immediate transfer to ice and washing with cold PBS. Cultures were then incubated with the myc monoclonal antibody for 2 hours at 4°C to label GLUT4 at the plasma membrane. Cells were subsequently washed with cold PBS on ice and then warmed at 37°C for 15 minutes in the presence or absence of 100 nM insulin. The reaction was stopped by chilling cultures on ice and washing extensively with cold PBS. Incubation with of phycoerythrin (PE)-conjugated donkey $F(ab')_2$ anti-mouse IgG secondary antibody followed for 1 hour. The extent of disappearance of GLUT4myc from the cell surface was compared to cells continually incubated on ice. After both steady state and internalization experiments, cells were again washed three times and gently scraped in PBS containing 4% BSA. Flow cytometric acquisitions were performed using a four-color FACSCalibur (BD Biosciences, Mountain View, CA). Side scatter (SSC), forward scatter (FSC) and PE outputs were collected in list-mode form and analyzed with FloJo (Treestar, Ashland, OR). All values are normalized to mock transfected cultures for at least 10,000 live cell events.

Fluorescence microscopy

Subsequent to treatments, cells were washed with PBS and fixed in 4% paraformaldehyde for 10 minutes on ice followed by 10 minutes at room temperature

(RT). Cells were then incubated with 0.1% Triton X-100 for 5 minutes, followed by washing and blocking in 1% BSA at RT. Primary incubations were performed for CIP4 and GLUT4 at concentrations of 1:200 in 400 μl of 1% BSA overnight at 4°C. Next, monolayers were washed and incubated with Cy3 anti-mouse and Cy5 anti-rabbit secondary antibodies (Invitrogen) for 1 hour at RT. Coverslips were mounted with ProLong Anti-Fade (Invitrogen). For plasmid expression studies, cells were fixed as described above under the appropriate insulin treatment and mounted with a coverslip. Muscle tissue was isolated from four age- and sex-matched mice (n=2). Wild-type mice were fasted for overnight, glucose-challenged for 25 minutes and sacrificed to isolate the muscle groups for sectioning. Extensor Digitorum Longus muscles were frozen in liquid-nitrogen cooled isopentane, and stored at –80°C. Muscles were then mounted using OTC and serially sectioned (8 μm) perpendicular to the axis of the EDL using a Microm 505M cryostat. Sections were then placed onto superfrost slides and immunohistochemically stained for CIP4 and GLUT4. Images were captured with a Zeiss LSM510 confocal microscope and composite images prepared with the LSM510 software package.

Transferrin internalization

Bovine holo-transferrin (Invitrogen) was labeled with ^{125}I (GE Radiochemicals), using IODO-BEADS (Pierce Biotechnology) according to the manufacturer protocols. RNAi-treated L6 GLUT4myc cells were depleted of transferrin by washing with serum-free growth media for 1-2 hours at 37°C. After starvation, cultures were exposed to a saturating concentration (5 μg/ml) of ^{125}I-labeled transferrin for the indicated times. After the indicated time-points, plates were removed, placed on ice and washed six times with cold, neutral pH buffer (150 mM NaCl, 5 mM KCl, 1 mM $CaCl_2$, 1 mM $MgCl_2$, 20 mM HEPES). Monolayers were then incubated with pH 2.0 buffer (500 mM NaCl, 0.2 N acetic acid) for 5 minutes at 4°C. The pH 2.0 buffer was then discarded and wells washed with neutral pH buffer three more times. Monolayers were then lysed in 0.05% SDS and 0.1% Triton-X100 and scraped. Incorporated ^{125}I-transferrin was measured by gamma counter and normalized to total protein content. Non-specific, cell-associated ^{125}I-transferrin was assessed in parallel by exposing cells to 5 μg/ml ^{125}I-labeled transferrin in the presence of a 200-fold excess of unlabeled holo-transferrin.

apFRET studies

apFRET was applied to quantify the extent and compartmental interactions between CIP4 and Dynamin-2 and between CIP4 and N-WASp. All images were recorded using a Zeiss LSM 510 laser scanning confocal microscope using a 63×, 1.3 NA objective. apFRET was applied largely as described previously where bleach settings are defined empirically (Greeson et al., 2006; Karpova et al., 2003). Briefly, a cell expressing any combination of YFP and CFP detailed in supplementary material Table S2 was selected and four regions of interest (ROIs) drawn for YFP bleaching and controls. The large ROI (ROI 3) was scanned ten times using routine scanning settings (supplementary material Table S2). The bleach ROIs for membrane (ROI 1) and cytosolic (ROI 2) regions was then bleached at 100% intensity for 1000 iterations or approximately 3 minutes. One ROI (ROI 4) was drawn to measure any potential for off-target bleaching, which accounted for less than 1% changes in YFP and CFP. Following the bleach, ten more scans were taken using the prebleach settings. The FRET efficiency (increase in CFP upon YFP bleaching) was calculated by the following equation:

$$\eta_{FRET} = 1 - \frac{I_{CFP,initial}}{I_{CFP,after\ photobleaching}} . \quad (1)$$

Furthermore, the distance between fluorophores was calculated by solving the equation for r:

$$\eta_{FRET} = \frac{R_0^6}{R_0^6 + r^6} , \quad (2)$$

where R_0, the distance at which 50% energy transfer takes place between YFP and CFP, is 4.87 nm (Bastiaens and Jovin, 1996).

Statistical analysis

Statistical analysis of the differences between discrete treatments was performed with using the Student's t-test for transferrin endocytosis and traffic, glucose uptake and GLUT4myc flow cytometric analysis. All tests were carried out at the 95% confidence interval using Microsoft Excel and JMP-IN 5.1.2 (SAS, Cary, NC) software packages.

This work was supported by a Grant-in-Aid from the American Heart Association, Charlotte Geyer Foundation, and NIH R01HL080052 to S.J.C. The authors also wish to acknowledge funding from UT-MD Anderson Cancer Center Odyssey Fellowship and the TN Law Foundation (S.M.H.), NIH 5T32CA009598 (to Bradley W. McIntyre supporting S.M.H.), NIH DC008134 (R.M.R.) and NSF BES044379 (R.M.R.). Additionally, we acknowledge funding from the Canadian Institutes of Health (Grant MT7307) to Amira Klip. The authors graciously thank Phil Bilan (Klip laboratory) for provision of the L6 myoblasts stably expressing the GLUT4myc epitope and for helpful discussions. The authors also thank Bradley McIntyre (Immunology, MDACC) for preparing the initial polyclonal and monoclonal antibodies to CIP4, Robert Langley (Cancer Biology, MDACC) for access to the LSM510, and K.K. Balasubramanian (Cancer Biology, MDACC) for assistance with iodinated transferrin studies. Deposited in PMC for release after 12 months.

The authors declare no competing interests. This work was supported by grants from the NIH HL80052, American Heart Association and the Charlotte Geyer Foundation. Deposited in PMC for release after 12 months.

References

Al-Hasani, H., Hinck, C. S. and Cushman, S. W. (1998). Endocytosis of the glucose transporter GLUT4 is mediated by the GTPase dynamin. *J. Biol. Chem.* **273**, 17504-17510.

Antonescu, C. N., Diaz, M., Femia, G., Planas, J. V. and Klip, A. (2008). Clathrin and non-clathrin mediated GLUT4 endocytosis in myocytes: effect of mitochondrial uncoupling. *Traffic* **9**, 1173-1190.

Aspenstrom, P. (1997). A Cdc42 target protein with homology to the non-kinase domain of FER has a potential role in regulating the actin cytoskeleton. *Curr. Biol.* **7**, 479-487.

Badour, K., McGavin, M. K., Zhang, J., Freeman, S., Vieira, C., Filipp, D., Julius, M., Mills, G. B. and Siminovitch, K. A. (2007). Interaction of the Wiskott-Aldrich syndrome protein with sorting nexin 9 is required for CD28 endocytosis and cosignaling in T cells. *Proc. Natl. Acad. Sci. USA* **104**, 1593-1598.

Bastiaens, P. I. H. and Jovin, T. M. (1996). Microspectroscopic imaging tracks the intracellular processing of a signal transduction protein: fluorescent-labeled protein kinase C beta I. *Proc. Natl. Acad. Sci. USA* **93**, 8407-8412.

Blot, V. and McGraw, T. E. (2006). GLUT4 is internalized by a cholesterol-dependent nystatin-sensitive mechanism inhibited by insulin. *EMBO J.* **25**, 5648-5658.

Bogan, J. S., McKee, A. E. and Lodish, H. F. (2001). Insulin-responsive compartments containing GLUT4 in 3T3-L1 and CHO cells: Regulation by amino acid concentrations. *Mol. Cell. Biol.* **21**, 4785-4806.

Chang, L., Adams, R. D. and Saltiel, A. R. (2002). The TC10-interacting protein CIP4/2 is required for insulin-stimulated Glut4 translocation in 3T3L1 adipocytes. *Proc. Natl. Acad. Sci. USA* **99**, 12835-12840.

Chang, L., Chiang, S. H. and Saltiel, A. R. (2004). Insulin signaling and the regulation of glucose transport. *Mol. Med.* **10**, 65-71.

Chang, L., Chiang, S. H. and Saltiel, A. R. (2007). TC10alpha is required for insulin-stimulated glucose uptake in adipocytes. *Endocrinology* **148**, 27-33.

Dombrosky-Ferlan, P., Grishin, A., Botelho, R. J., Sampson, M., Wang, L., Rudert, W. A., Grinstein, S. and Corey, S. J. (2003). Felic (CIP4b), a novel binding partner with the Src kinase Lyn and Cdc42, localizes to the phagocytic cup. *Blood* **101**, 2804-2809.

Dugani, C. B. and Klip, A. (2005). Glucose transporter 4, cycling, compartments, and controversies. *EMBO Rep.* **6**, 1137-1142.

Greeson, J. N., Organ, L. E., Pereira, F. A. and Raphael, R. M. (2006). Assessment of prestin self-association using fluorescence resonance energy transfer. *Brain Res.* **1091**, 140-150.

Hall, A. (1998). Rho GTPases and the actin cytoskeleton. *Science* **279**, 509-514.

Henne, W. M., Kent, H. M., Ford, M. G., Hegde, B. G., Daumke, O., Butler, P. J., Mittal, R., Langen, R., Evans, P. R. and McMahon, H. T. (2007). Structure and analysis of FCHo2 F-BAR domain: a dimerizing and membrane recruitment module that effects membrane curvature. *Structure* **15**, 839-852.

Higgs, H. N. and Pollard, T. D. (2001). Regulation of actin filament network formation through Arp2/3 complex: activation by a diverse array of proteins. *Annu. Rev. Biochem.* **70**, 649-676.

Ho, H. Y., Rohatgi, R., Lebensohn, A. M., Le M., Li, J., Gygi, S. P. and Kirschner, M. W. (2004). Toca-1 mediates Cdc42-dependent actin nucleation by activating the N-WASP-WIP complex. *Cell* **118**, 203-216.

Icking, A., Matt, S., Opitz, N., Wiesenthal, A., Muller-Esterl, W. and Schilling, K. (2005). NOSTRIN functions as a homotrimeric adaptor protein facilitating internalization of eNOS. *J. Cell Sci.* **118**, 5059-5069.

Ishikura, S. and Klip, A. (2008). Muscle cells engage Rab8A and myosin Vb in insulin-dependent GLUT4 translocation. *Am. J. Physiol. Cell Physiol.* **295**, C1016-C1025.

Itoh, T. and De Camilli, P. (2006). BAR, F-BAR (EFC) and ENTH/ANTH domains in the regulation of membrane-cytosol interfaces and membrane curvature. *Biochim. Biophys. Acta* **1761**, 897-912.

Itoh, T., Erdmann, K. S., Roux, A., Habermann, B., Werner, H. and De Camilli, P. (2005). Dynamin and the actin cytoskeleton cooperatively regulate plasma membrane invagination by BAR and F-BAR proteins. *Dev. Cell* **9**, 791-804.

Jiang, Z. Y., Chawla, A., Bose, A., Way, M. and Czech, M. P. (2002). A phosphatidylinositol 3-kinase-independent insulin signaling pathway to N-WASP/Arp2/3/F-actin required for GLUT4 glucose transporter recycling. *J. Biol. Chem.* **277**, 509-515.

Kakimoto, T., Katoh, H. and Negishi, M. (2006). Regulation of neuronal morphology by Toca-1, an F-BAR/EFC protein that induces plasma membrane invagination. *J. Biol. Chem.* **281**, 29042-29053.

Kamioka, Y., Fukuhara, S., Sawa, H., Nagashima, K., Masuda, M., Matsuda, M. and Mochizuki, N. (2004). A novel dynamin-associating molecule, formin-binding protein 17, induces tubular membrane invaginations and participates in endocytosis. *J. Biol. Chem.* **279**, 40091-40099.

Karpova, T. S., Baumann, C. T., He, L., Wu, X., Grammer, A., Lipsky, P., Hager, G. L. and McNally, J. G. (2003). Fluorescence resonance energy transfer from cyan to yellow fluorescent protein detected by acceptor photobleaching using confocal microscopy and a single laser. *J. Microsc.* **209**, 56-70.

Kessels, M. M. and Qualmann, B. (2002). Syndapins integrate N-WASp in receptor-mediated endocytosis. *EMBO J.* **21**, 6083-6094.

Leprince, C., Le Scolan, E., Meunier, B., Fraisier, V., Brandwon, N., De Gunzburg, J. and Camonis, J. (2003). Sorting nexin 4 and amphiphysin 2, a new partnership between endocytosis and intracellular trafficking. *J. Cell Sci.* **116**, 1937-1948.

Lodhi, I. J., Chiang, S. H., Chang, L., Vollenweider, D., Watson, R. T., Inoue, M., Pessin, J. E. and Saltiel, A. R. (2007). Gapex-5, a Rab31 guanine nucleotide exchange factor that regulates Glut4 trafficking in adipocytes. *Cell Metab.* **5**, 59-72.

Lundmark, R. and Carlsson, S. R. (2003). Sorting nexin-9 participates in clathrin-mediated endocytosis through interactions with the core components. *J. Biol. Chem.* **278**, 46772-46781.

Merrifield, C. J., Feldman, M. E., Wan, L. and Almers, W. (2002). Imaging actin and dynamin recruitment during invagination of single clathrin-coated pits. *Nat. Cell Biol.* **4**, 691-698.

Merrifield, C. J., Perrais, D. and Zenisek, D. (2005). Coupling between clathrin-coated-pit invagination, cortactin recruitment, and membrane scission observed in live cells. *Cell* **121**, 593-606.

Moyers, J. S., Bilan, P. J., Reynet, C. and Kahn, C. R. (1996). Overexpression of rad inhibits glucose uptake in cultured muscle and fat cells. *J. Biol. Chem.* **271**, 23111-23116.

Robinson, L. J., Pang, S. H., Harris, D. S., Heuser, J. and James, D. E. (1992). Translocation of the glucose transporter (Glut4) to the cell-surface in permeabilized 3T3-L1 adipocytes – effects of ATP, insulin, and GTP-Gamma-S and localization of Glut4 to clathrin lattices. *J. Cell Biol.* **117**, 1181-1196.

Su, X., Kong, C. and Stahl, P. D. (2007). Gapex-5 mediates ubiquitination, trafficking, and degradation of epidermal growth factor receptor. *J. Biol. Chem.* **282**, 21278-21284.

Tian, L., Nelson, D. L. and Stewart, D. M. (2000). Cdc42-interacting protein 4 mediates binding of the Wiskott-Aldrich syndrome protein to microtubules. *J. Biol. Chem.* **275**, 7854-7861.

Traer, C. J., Rutherford, A. C., Palmer, K. J., Wassmer, T., Oakley, J., Attar, N., Carlton, J. G., Kremerskothen, J., Stephens, D. J. and Cullen, P. J. (2007). SNX4 coordinates endosomal sorting of TfnR with dynein-mediated transport into the endocytic recycling compartment. *Nat. Cell Biol.* **9**, 1370-1380.

Tsujita, K., Suetsugu, S., Sasaki, N., Furutani, M., Oikawa, T. and Takenawa, T. (2006). Coordination between the actin cytoskeleton and membrane deformation by a novel membrane tubulation domain of PCH proteins is involved in endocytosis. *J. Cell Biol.* **172**, 269-279.

Volchuk, A., Narine, S., Foster, L. J., Grabs, D., De Camilli, P. and Klip, A. (1998). Perturbation of dynamin II with an amphiphysin SH3 domain increases GLUT4 glucose transporters at the plasma membrane in 3T3-L1 adipocytes. *J. Biol. Chem.* **273**, 8169-8176.

Wang, L., Rudert, W. A., Grishin, A., Dombrosky-Ferlan, P., Sullivan, K., Deng, X., Whitcomb, D. and Corey, S. (2002). Identification and genetic analysis of human and mouse activated Cdc42 interacting protein-4 isoforms. *Biochem. Biophys. Res. Commun.* **293**, 1426-1430.

Wang, Q. H., Khayat, Z., Kishi, K., Ebina, Y. and Klip, A. (1998). GLUT4 translocation by insulin in intact muscle cells: detection by a fast and quantitative assay. *FEBS Lett.* **427**, 193-197.

Watson, R. T., Khan, A. H., Furukawa, M., Hou, J. C., Li, L., Kanzaki, M., Okada, S., Kandror, K. V. and Pessin, J. E. (2004). Entry of newly synthesized GLUT4 into the insulin-responsive storage compartment is GGA dependent. *EMBO J.* **23**, 2059-2070.

Weaver, A. M., Karginov, A. V., Kinley, A. W., Weed, S. A., Li, Y., Parsons, J. T. and Cooper, J. A. (2001). Cortactin promotes and stabilizes Arp2/3-induced actin filament network formation. *Curr. Biol.* **11**, 370-374.

Wigge, P., Vallis, Y. and McMahon, H. T. (1997). Inhibition of receptor-mediated endocytsis by the amphiphysin SH3 domain. *Curr. Biol.* **7**, 554-560.

Journal of Cell Science

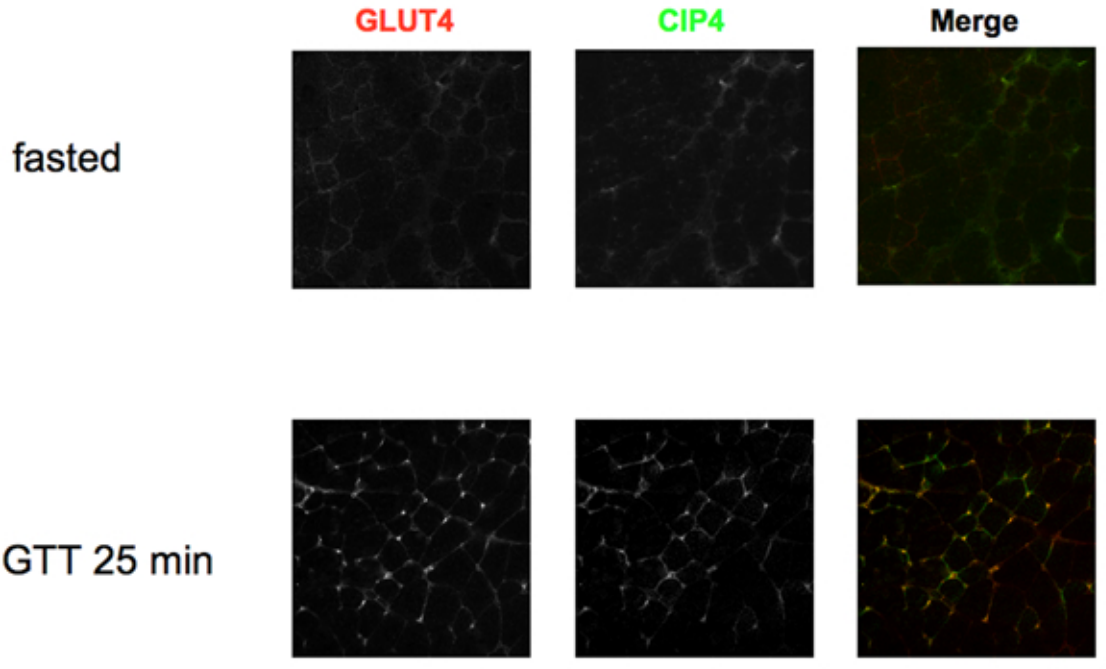
GLUT4
CIP4
Merge
fasted
GTT 25 min

Table S1. PCR primers applied for qPCR analysis in L6 GLUT4myc myoblasts

	Forward	Reverse
Actin	TGTCACCAACTGGGACGATA	ACCCTCATAGATGGGCACAG
CIP4a	AACCGAGAGTTGCAGAAGGA	ATCAGGTGGGGCAGTAGTTG
CIP4h	GAGCAGCTTCCAGCCGTAG	CTCGCTCAGTATGGCCAAG
FBP17	CCGACATCAATGTGACCAAG	TATACCGTCCAGGCACTTCC
Toca1	ACCAGAGCAGAGGCGTAAGA	ACACCTGTTTTGCCTTCCAC

Table S2. apFRET data collection settings

	Image settings		**Bleach settings**
	CFP	YFP	YFP
Laser power	80%	80%	80%
Transmission %	30%	30%	100%
Scan speed	9	9	9
Pixel drift (μs)	1.60	1.60	1.60
Detector gain	800-1000	400-600	-